Measurement of NMR flow propagators and local numerical analysis of dual scale porous media

Yong Zheng,[1] *Igor Shikhov,*[1] *Marcel N. d'Eurydice,*[1,2] *Christoph Arns*[1]

[1] The University of New South Wales, Australia
[2] Victoria University of Wellington, New Zealand

Corresponding author: Christoph Arns, School of Petroleum Engineering, the University of New South Wales, NSW 2052, E-Mail: c.arns@unsw.edu.au

Abstract

Flow propagators have been frequently used in characterisation of porous media and the study of fluid transport behaviour. Previous work considered the shape of measured flow propagators using Nuclear Magnetic Resonance (NMR) discussed the influence of pore geometry, dispersion, relaxation and internal gradients. In addition, numerically simulated flow propagators were also reported. However, a quantitative numerical analysis of local contributions to flow propagators has not been considered in the literature, yet may provide significant new insights into the flow behaviour through complex porous media. In this work we use two types of beads to realize a dual-scale bead pack consisting of micro- and macro-pore regions for the NMR experiments. A low-field NMR system (2 MHz) was used to measure flow propagators for this sample. We further generated a dual-scale Gaussian Random Field (GRF) image based on porosity, beads diameters and volume fraction of each type of bead for numerical simulations. A Lattice Boltzmann Method (LBM) and Random Walk (RW) technique were combined to derive the simulated flow propagators and validated against experiments. We carry out a local analysis of the flow propagators showing a significant difference in bandwidth of displacements in micro- and macro-pore regions. In addition, the local flow propagators indicate a linear relationship between mixing (the fluid exchange on regions' boundaries) and flow velocities as well as a non-linear correlation between mixing and evolution times.

Keywords

NMR, flow propagator, dual scale model, local analysis

1. Introduction

NMR flow propagators measure the probability distribution of displacement. The are widely used in porous media characterisation and flow behaviour research, which can benefit many areas, such as the oil industry, groundwater engineering, waste management, carbon capture and sequestration. Over the past two decades, Scheven et al. (2004) [1], Packer et al.

(1998) [2], Johns et al. (2003) [3], measured flow propagators for fluids in bead packs, sandstones and carbonates and comprehensively discussed how pore geometry and other effects, e.g. relaxation and internal gradient, affect the shape of flow propagators. Transport behaviour, especially dispersion had also been studied by many researchers [4-6]. A variety of propagator-based techniques have been developed, including low field NMR flow propagator [7], 2D flow propagator [8], rapid measurement of flow propagator [9] and T_2-resolved flow propagator [10], all of which make it an attractive and powerful tool to characterise flow in porous media. Single-phase flow propagators were simulated numerically [11-12].

The spatially-resolved or local propagators are potentially a sensitive probe to the connectivity of different morphological units of a heterogeneous sample and thus very useful for the characterisation of their transport properties; however, an experimental implementation is complicated. This might be the reason why numerically simulated local propagators have not been reported. In this work, we successfully simulated local flow propagators in a dual-scale bead pack represented by a digitized model. Numerical results were validated by matching experimental and simulated global flow propagators.

2. Experiments

A bead pack sample made of two types of beads (mean diameters are 0.5 and 1.5 *mm*) was studied. These two types of beads were packed in clusters to generate distinctive regions with different pore sizes inside a tube of 3 *cm* in diameter, 5 *cm* in length. The total volumes of each kind of bead are the same. We measured the weight difference between dry and 100% water saturated sample, and the weight of water in pores corresponds to the volume of 52 cm^3 in the total cylindrical volume of 141.37 cm^3. So the measured average porosity is 37%.

All NMR flow propagator measurements were performed on a 2 MHz Magritek Rock Core Analyzer. A schematic of the pulse sequence used is shown in Fig. 1.

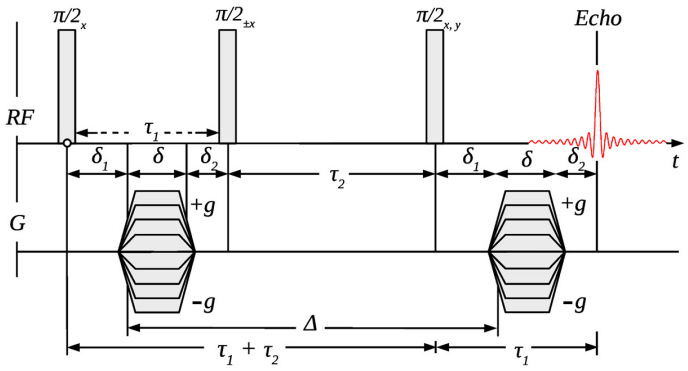

Fig. 1: Pulsed gradient stimulated echo (PGSTE) NMR sequence used for flow propagator measurements

The first 90° pulse tips the magnetization to the transverse plane, and then a pulsed gradient field is applied to imprint the initial position distribution onto the phase space of the magnetization. Subsequently, a second 90° pulse is applied to store the phase information on the longitudinal direction for a period τ_2. A final 90° pulse is then applied to bring the stored magnetization back to the transverse plane followed by a refocusing pulsed gradient field to generate an echo.

The difference of the spin positions ($\vec{r}_i$) at the first and second gradient pulses produces an accumulated phase given by

$$\varphi_i(\Delta) = \gamma \vec{g} \delta [\vec{r}_i(\Delta) - \vec{r}_i(0)] = \gamma \vec{g} \delta [\vec{R}_i(\Delta)], \quad (1)$$

which is the phase shift of the i-th spin that moved a distance $\vec{R}_i(\Delta)$ along the direction of the applied gradients' $\vec{g}$. In Eq. (1) γ is the gyromagnetic ratio, and δ denotes the duration of applied gradients.

The amplitude of the echo is measured for a set of gradient intensities from –g to +g and flow propagator $P_\Delta(\vec{R})$ is obtained from a Fourier transformation of all echo amplitudes as function of the gradient intensity [13-14]:

$$s_\Delta(\vec{q}) = \int P_\Delta(\vec{R}) e^{i2\pi q \cdot \vec{R}(\Delta)} d\vec{R}\,, \tag{2}$$

where $\vec{q} = \gamma\vec{g}\delta/(2\pi)$, and it is also known as magnetization wave vector.

3. Simulations

3.1. Modelling the dual scale pore structure

We created a 3D digitised representation of the dual scale bead pack system used for lab measurements. The resulting model acknowledges bead size, porosity and volumetric fraction of each type of bead. We employed the Gaussian Random Field (GRF) approach to generate the boundaries between phase clusters, constraining the volume of each phase by experimental data. These two phases were seeded with spheres of 5 voxels and 15 voxels in diameter respectively following a Poisson process [15], resulting in four phases – solid and fluid in each of the macro-porous and micro-porous regions.

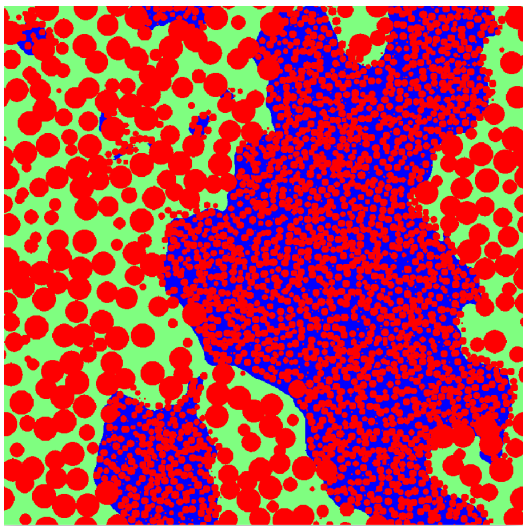

Fig. 2: A slice through GRF dual scale bead pack model image of 800^3 voxels, where the pore space of different scales received separate labels and both all beads are labelled similarly (for solid).

3.1. Generation of velocity field

The velocity field was generated from a single phase flow Lattice Boltzmann Method (LBM) solver. This method has proved very successful in simulating fluid flow though porous media [12]. In this simulation we used a D3Q19 lattice, corresponding to 3 dimensions and 19 velocity vectors [16]. The flow direction was the same as in experiments. The LBM simulation generates a velocity field with mean velocity of 1, calculated for the case of laminar flow. When we simulate flow propagators, the velocity field is then scaled to the mean velocity of experimental measurements.

3.2. Simulation of flow propagators

The GRF dual scale image was seeded with 800^3 particles, thus one particle in every voxel, and all particles (representing fluids) were initially sited at the central point of their voxels. Convection-diffusion was applied as the transport model. For each time step dt, the displacements of convection $\vec{d}_c$ were calculated from the velocity field

$$\vec{d}_c = dt * \vec{v}(x,y,z), \tag{3}$$

where $\vec{v}(x,y,z)$ is a velocity vector for particles at the position (x,y,z). Then we used a random walk method to simulate diffusion. In 3D simulation, the displacements due to diffusion d_d is calculated by

$$d_d = \sqrt{6Ddt}\ , \tag{4}$$

where D is the self-diffusion coefficient of fluid. The direction of d_d is randomly chosen from 6 directions in 3D grids. We apply no-slip boundary conditions at the fluid-solid interphase. After a total time period of Δ, we plotted the displacement distribution, thus flow propagator.

In addition, we tracked the movement of fluids as well as their residence time in different phases for local numerical analysis.

4. Results

4.1. Global flow propagators

Fig. 3 shows the flow propagator measurements and simulations at different evolution times. The shape of the simulated flow propagators at different displacement times is similar to the experimentally observed propagators. Furthermore, mean displacements between simulations and experiment are within 5%. This suggests that the generated GRF image is representative for the dual scale bead pack and that the propagator simulations based on it are accurate.

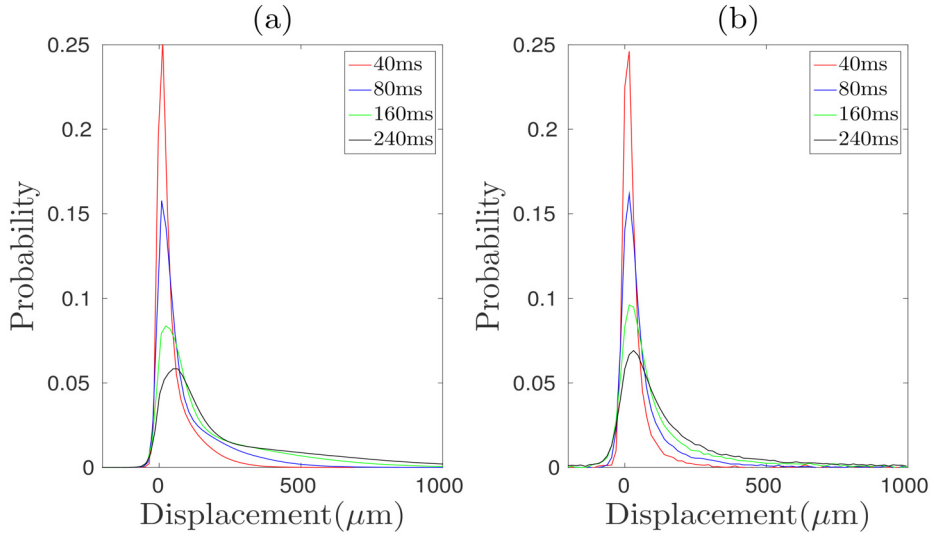

Fig.3: (a) Simulation of flow propagators on a dual scale GRF image. (b) NMR measurements of flow propagators of dual scale bead pack.

4.2. Local flow propagators

We extract local information from our simulation, which cannot be accessed from the experimental measurements used in this work. Micro- and macro-pore regions were given separate labels and we tracked the position of random walkers and time they stayed within each region. The acquired displacement information enables us to calculate local flow propagators (Fig. 4).

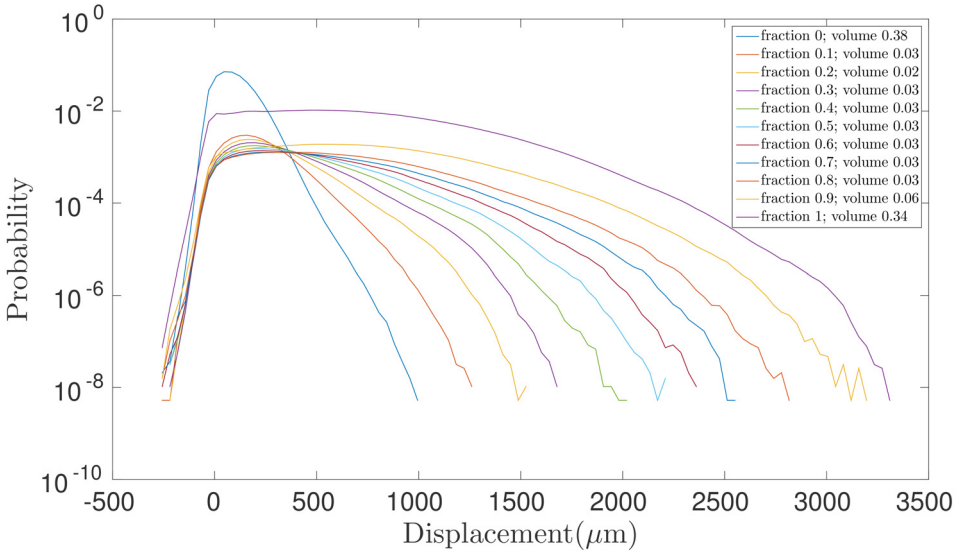

Fig.4: Local flow propagators at mean velocity 1842 *μm/s,* displacement time 240 *ms*. Time fraction indicates the time one particle stays in macro pore regions. The legend also shows the volume of particles of a certain time fraction.

As shown in Fig. 4, the bandwidth of flow propagator calculated for the micro-pore region (time fraction equals 0) is much narrower than in the macro-pore region (time fraction equals 1), which directly illustrates the permeability difference of micro and macro pore regions. For particles which crossed region boundaries (time fraction ranging from 0.1 to 0.9), the bandwidths of their flow propagators sits in-between and the volume is relatively small at this displacement time and global mean flow velocity.

Varying mean velocities and displacement times, we calculated the total mixing volume (sum up all mixing volumes of time fraction ranging from 0.1 to 0.9) for all scenarios (Table 1).

Table 1: Mixing fraction at different velocities and various displacement times

Velocity \ Time	40 *ms*	80 *ms*	160 *ms*	320 *ms*
0 *μm/s*	0.038	0.052	0.071	0.097
574 *μm/s*	0.045	0.068	0.107	0.170
1151 *μm/s*	0.058	0.094	0.153	0.253
1842 *μm/s*	0.074	0.123	0.206	0.341

Table 1 illustrates that the mixing fraction increases with time and mean flow velocity. We plotted the data of Table 1 to study the influence of time and velocity on the mixing volume separately. At fixed displacement time, mixing content increases linearly with velocity, while at fixed velocity, the mixing content has a non-linear correlation with time (Fig. 5).

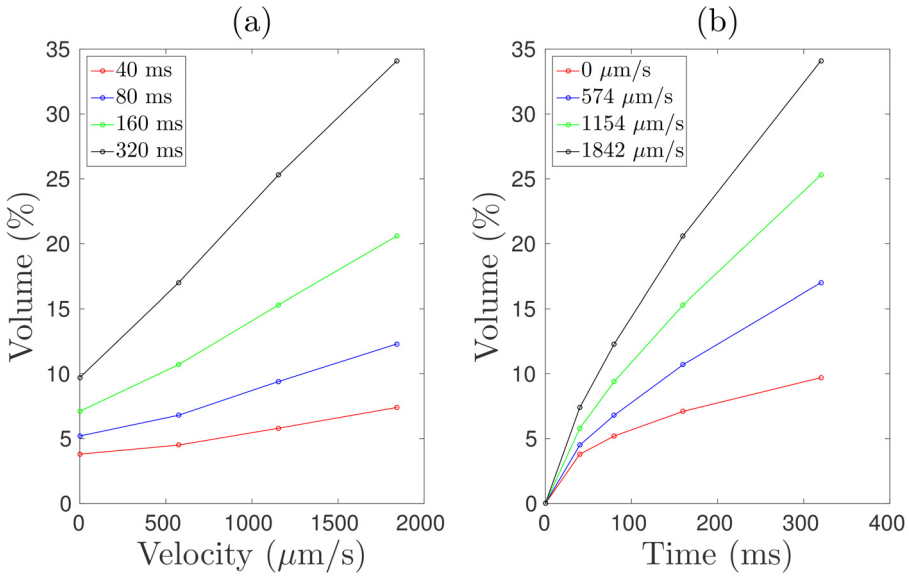

Fig.5: (a) Correlation between mixing volume and mean velocity at various displacement times; (b) Correlation between mixing volume and observation time at various velocities.

Mixing may occur due to either convection flow or diffusion. At a fixed observation time, the contribution to mixing fractions from diffusion can be assumed constant, and these fractions are plotted in Fig. 5(a), where the velocity equals 0 μm/s. In the same plot, the mixing volume increases almost linearly with velocity increase, indicating a major contribution from convection flow at higher velocities, otherwise it should be a non-linear line due to diffusion effects. This can be proved from the data points where the velocity is smaller than 574 μm/s (corresponding Peclet number for the sample is 260). These points deviate from the straight line for low velocities because diffusion is dominant. To further illustrate this behaviour, we plot the same data in a different way in Fig. 5(b). For each given fixed mean velocities, a non-linear correlation between mixing volume and observation time is observed. Higher velocities reduce the influence of diffusion, so the curve transforms gradually from a non-linear shape for pure diffusion (red line) to more linear-like shapes at higher mean velocities.

5. Conclusions

Numerical simulations based on GRF image agree well with the experimental NMR flow propagator measurements, indicating that the generated dual-scale system is representative. Local analysis shows the significant difference in bandwidth of propagators in micro-pore and macro-pore regions, which is expected. Interestingly, the transport phenomenon on regions' boundaries suggests that the mixing volume increases linearly with mean velocity and holds a non-linear correlation with evolving time. It is worth mentioning that both experiments and simulations were conducted in limited observation times where the measurements are not significantly affected by T1 and T2 relaxations. Further study may be done for longer observation times. The mixing volume may converge to a certain value less than 1, indicating a high flow rate path. Otherwise, given long enough time, the fluids at macro-pore and micro-pore regions may be fully mixed at a critical velocity. However, it requires a proper experiment to ground this prediction.

References

[1] Scheven, U. M., et al. "NMR propagator measurements on flow through a random pack of porous glass beads and how they are affected by dispersion, relaxation, and internal field inhomogeneities." *Physical Review E* 69.2 (2004): 021201.

[2] Packer, K. J., et al. "The characterisation of fluid transport in porous solids by means of pulsed magnetic field gradient NMR." *Magnetic Resonance Imaging* 16.5 (1998): 463-469.

[3] Johns, M. L., et al. "Using MR techniques to probe permeability reduction in rock cores." *AIChE Journal* 49.5 (2003): 1076-1084.

[4] Codd, S. L., et al. "Taylor dispersion and molecular displacements in Poiseuille flow." *Physical Review E* 60.4 (1999): R3491.

[5] Manz, B., et al. "Flow and dispersion in porous media: Lattice Boltzmann and NMR studies." *AIChE Journal* 45.9 (1999): 1845-1854.

[6] Seymour, Joseph D., and Paul T. Callaghan. "Generalized approach to NMR analysis of flow and dispersion in porous media." *AIChE* Journal 43.8 (1997): 2096-2111.

[7] Singer, P. M., et al. "Low magnetic fields for flow propagators in permeable rocks." *Journal of Magnetic Resonance* 183.2 (2006): 167-177.

[8] Stapf, S., et al. "Two-dimensional nuclear magnetic resonance measurements and numerical simulations of fluid transport in porous rocks." *Physics of Fluids* 12.3 (2000): 566-580.

[9] Mitchell, J., et al. "A rapid measurement of flow propagators in porous rocks." *Journal of Magnetic Resonance* 191.2 (2008): 267-272.

[10] Britton, M. M., et al. "NMR relaxation and pulsed field gradient study of alginate bead porous media." *Journal of Magnetic Resonance* 169.2 (2004): 203-214.

[11] Hussain, R., et al. "Monitoring water transport in sandstone using flow propagators: A quantitative comparison of nuclear magnetic resonance measurement with lattice Boltzmann and pore network simulations." *Advances in Water Resources* 60 (2013): 64-74.

[12] Maier, R. S., et al. "Simulation of flow through bead packs using the lattice Boltzmann method." *Physics of Fluids* 10.1 (1998): 60-74.

[13] Kärger, J., et al. "The propagator representation of molecular transport in microporous crystallites." *Journal of Magnetic Resonance* 51.1 (1983): 1-7.

[14] Callaghan, Paul T. *Translational dynamics and magnetic resonance: principles of pulsed gradient spin echo NMR*. Oxford University Press, 2011.

[15] Arns, C. H., et al. "Euler-Poincaré characteristics of classes of disordered media." *Physical Review E* 63.3 (2001): 031112.

[16] Kang, Q. J., et al. "Displacement of a three-dimensional immiscible droplet in a duct." *Journal of Fluid Mechanics* 545 (2005): 41-66.